ORNL/TM-7360

ornl

OAK RIDGE NATIONAL LABORATORY

UNION CARBIDE

Calculation of Neutron and Gamma Ray Energy Spectra for Fusion Reactor Shield Design: Comparison with Experiment

R. T. Santoro
R. G. Alsmiller, Jr.
J. M. Barnes
G. T. Chapman

OPERATED BY
UNION CARBIDE CORPORATION
FOR THE UNITED STATES
DEPARTMENT OF ENERGY

DISCLAIMER

Printed in the United States of America. Available from
National Technical Information Service
U.S. Department of Commerce
5285 Port Royal Road, Springfield, Virginia 22161
NTIS price codes—Printed Copy: A03; Microfiche A01

ORNL/TM-7360
Dist. Category UC-20d

Contract No. W-7405-eng-26

Engineering Physics Division

CALCULATION OF NEUTRON AND GAMMA RAY ENERGY SPECTRA FOR FUSION REACTOR SHIELD DESIGN: COMPARISON WITH EXPERIMENT*

R. T. Santoro
R. G. Alsmiller, Jr.
J. M. Barnes[+]
G. T. Chapman

Date Published - August 1980

*Submitted for Journal publication

[+]Computer Sciences Division

OAK RIDGE NATIONAL LABORATORY
Oak Ridge, Tennessee 37830
operated by
UNION CARBIDE CORPORATION
for the
DEPARTMENT OF ENERGY

THIS PAGE

WAS INTENTIONALLY

LEFT BLANK

ACKNOWLEDGEMENTS

The authors wish to thank E. M. Oblow for his comments and suggestions during the early phases of this analysis.

ABSTRACT

Integral experiments that measure the transport of ∿14 MeV D-T neutrons through laminated slabs of proposed fusion reactor shield materials have been carried out at the Oak Ridge National Laboratory. Measured and calculated neutron and gamma ray energy spectra are compared as a function of the thickness and composition of stainless steel type 304, borated polyethylene, and Hevimet (a tungsten alloy), and as a function of detector position behind these materials. The measured data were obtained using a NE-213 liquid scintillator using pulse-shape discrimination methods to resolve neutron and gamma ray pulse height data and spectral unfolding methods to convert these data to energy spectra. The calculated data were obtained using two-dimensional discrete ordinates radiation transport methods in a complex calculational network that takes into account the energy-angle dependence of the D-T neutrons and the nonphysical anomalies of the S_n method. The transport calculations incorporate ENDF/B-IV cross section data from the VITAMIN C data library. The measured and calculated neutron energy spectra are in good agreement behind slab configurations of stainless steel type 304 and borated polyethylene (∿10% for all neutron energies above 850 keV). When 5 cm of Hevimet is added to a 45-cm-thick SS-304 plus BP slab assembly, the agreement is less favorable. The agreement among the measured and calculated gamma ray spectra for energies above 750 keV ranges from ∿25% to a factor of ∿5 depending on the slab composition.

I. INTRODUCTION

The nuclear performance of the blanket and shield in a fusion reactor will have a significant impact on the overall operation and capital cost of the reactor. It is necessary, therefore, to have experimental verification of the nuclear data and radiation transport methods that will be used to carry out the nuclear design calculations. Integral experiments are being performed at the Oak Ridge National Laboratory to provide the experimental data needed for this verification. The experiments begin with measurements of the transport of $\sim$ 14 MeV neutrons through laminated slabs of materials that are anticipated for use in the blankets and shields of fusion reactors. The experimental program proceeds from attenuation measurements to the determination of the effects of neutron streaming through penetrations in these assemblies. These data will be important in assessing the effects on reactor performance of the penetrations through the blanket-shield assembly for neutron beam injection, rf heating, diagnostics, and evacuation.

The experiments are complemented by an analytic program that provides verification of the calculational methods and nuclear data by making extensive comparisons between the measured results and those obtained from calculation. The calculated data are obtained using the best available cross section data and the radiation transport codes that are most widely used in the fusion community for the nuclear analysis of reactor systems.

Measurements and calculations have been carried out to determine the transport of $\sim$ 14 MeV neutrons through laminated slabs of stainless steel type-304, borated polyethylene, and Hevimet (a tungsten alloy). A complete description of the experiment and compilations of the measured neutron and

gamma ray pulse-height spectra as a function of the slab thickness and composition and the detector position behind the slabs are given in Ref. 1. Also included in this document are the neutron and gamma ray energy spectra obtained by applying spectral unfolding methods to the pulse height data. In this paper, calculated neutron and gamma ray energy spectra are compared with those obtained from the measurements. The calculated results were obtained using two-dimensional discrete ordinates radiation transport methods with the experimental geometry represented in cylindrical geometry.

The details of the experimental configuration and the radiation detection system are described in Section II. The details of the calculation including a description of the calculational model of the experiment, radiation transport sequences, and the nuclear data are given in Section III. The measured and calculated neutron and gamma ray energy spectra are compared and discussed in Section IV.

II. DETAILS OF THE EXPERIMENT

The experimental facility for performing the integral measurements is shown in an artist's rendition in Fig. 1. The important components include an electrostatic generator, a tritium target-source can assembly, a concrete test slab support structure, the neutron and gamma ray detection system, and a thermal neutron shield.

Deuterons are accelerated in the generator to a kinetic energy of 250 keV and are focused on a 4 mg/cm^2 thick titanium-tritide target. The deuterons react with the tritium to produce ~14 MeV neutrons via the

$$D + T \rightarrow n + {}^4He + 17.6\ MeV \qquad (1)$$

reaction. The target is enclosed in a cylindrical, re-entrant iron can having

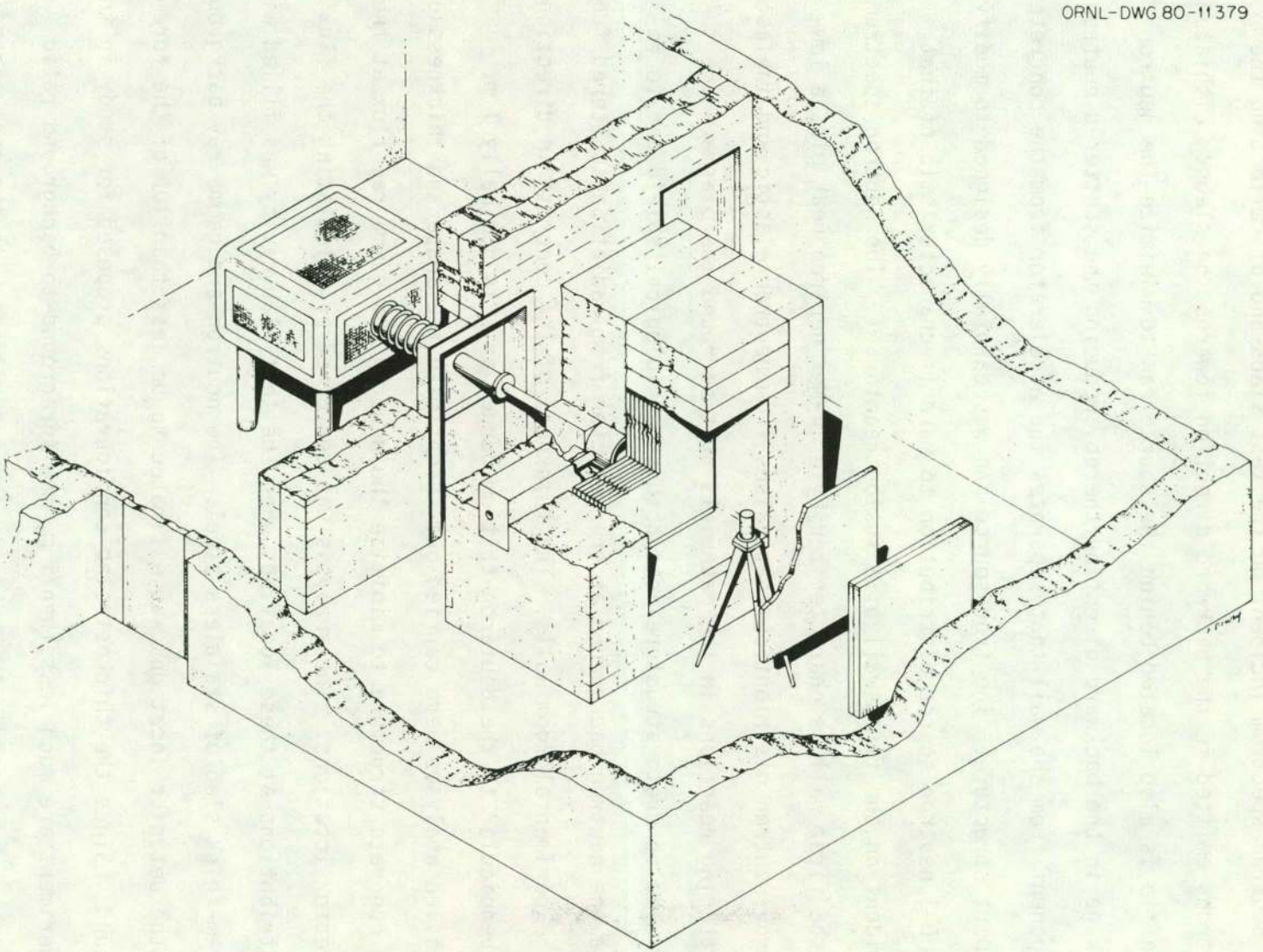

Fig. 1. Artist's rendition of the experimental facility.

a wall thickness of 7.5 cm. This can has the dual function of shaping the neutron spectrum incident on the test slabs and of reflecting the neutrons emitted in the backward direction towards the slabs. Lithiated paraffin is also located behind the source can to minimize the neutron leakage in the backward direction thereby reducing the scattered neutron component from the wall that separates the accelerator from the concrete support structure. The iron source can was carefully designed to modify the D-T neutron source distribution to make it characteristic of that incident on the first wall of a fusion reactor.[2,3] The neutron spectrum on the first wall is characterized by a 14-MeV neutron peak plus a low-energy neutron distribution that arises from neutron elastic and inelastic scattering reactions in the materials that surround the plasma.

The concrete structure acts both as a biological shield and to reduce the neutron background at the detector from radiation scattered from the experimental room walls. The thickness of the concrete in directions perpendicular to the deuteron tritium target axis is nominally 1 m. Detailed analyses were carried out to optimize the shape and thickness of the concrete structure to minimize the neutron and gamma ray flux at the detector locations. The analysis was performed by calculating the flux distributions at these locations when the test slab cavity was filled with a 1-m-thick slab of stainless steel. The neutron and gamma ray background at the detector locations was estimated to be less than 10% of the foreground. Since the thickest slab configurations proposed for study in the experiment are much less than 1 m, the foreground-to-background ratio would be correspondingly higher in the experiments with the test slabs in place.

These scoping studies also revealed a significant contribution to the background counting rates from a high thermal neutron flux emanating from the wall behind the detector. An iron slab was placed between the detector and the wall to reduce the intensity of the thermal neutron return from the wall. The distance from the detector to the slab was determined to be ∿50 cm for optimum shielding. Detailed descriptions of the experimental facility and the analyses to optimize the design of the concrete slab support structure may be found in Refs. 2 and 3.

The neutron-gamma-ray detector consisted of 66.1 g of NE-213 liquid scintillator contained in a cylindrical aluminum can having a wall thickness of 4.32×10^{-2} cm and coated on the inside with titanium oxide paint. The active volume of the detector is 79 cm^3 (4.658 cm dia. x 4.658 cm high). The scintillator was mounted on a RCA 8850 photomultiplier tube. Neutron and gamma ray events in the detector were separated using pulse shape discrimination methods and stored in separate memory locations in a ND-812 pulse height analyzer/computer. The pulse height data were transferred to a PDP-10 disk for storage and subsequent analysis. The neutron and gamma ray pulse height data were normalized to the absolute neutron yield from the target which was determined using associated particle counting methods.

For 250 keV incident deuterons, the neutrons from the D-T reaction are emitted isotropically in the center-of-mass system. The alpha particles produced in the reaction are emitted at 180° with respect to the neutron so that if the alpha particles counted are within a well-defined solid angle, the number of conjugate neutrons is known and the total neutron source strength can be determined from the kinematics of the reaction.

The pulse height data were obtained for neutrons with energies above 850 keV and for gamma rays above 750 keV. The dynamic range of the neutron pulse height distribution and the nonlinearity of light output from the scintillator limits the detection of neutrons to those with energies above 850 keV. The gamma ray pulse height was biased for energies above 750 keV although a somewhat broader energy range is possible since for gamma ray events the response of NE-213 is linear. The neutron and gamma ray pulse height spectra were unfolded using the program FERD[4] to produce energy spectra. The neutron response matrix was obtained using the pulsed neutron beam from the Oak Ridge Linear Accelerator[1] and the gamma ray response matrix was generated using gamma ray sources of known energies. The energy resolution of the detector varies as

$$R_N = \sqrt{300 + 800/E_N}$$

for neutrons of energy E_N and as

$$R_\gamma = \sqrt{170 + 288/E_\gamma}$$

for gamma rays of energy E_γ. R_N and R_γ are the full width of half maximum (in percent) of the detector response to neutrons or gamma rays, respectively. Figure 2 shows the response of the NE-213 detector to 14-MeV neutrons and Fig. 3 shows the response of the detector to the 1.37 and 2.76 MeV gamma rays from ^{24}Na. In Fig. 2, and all of the measured curves given below, the two curves indicate the statistical uncertainty in the unfolded results.

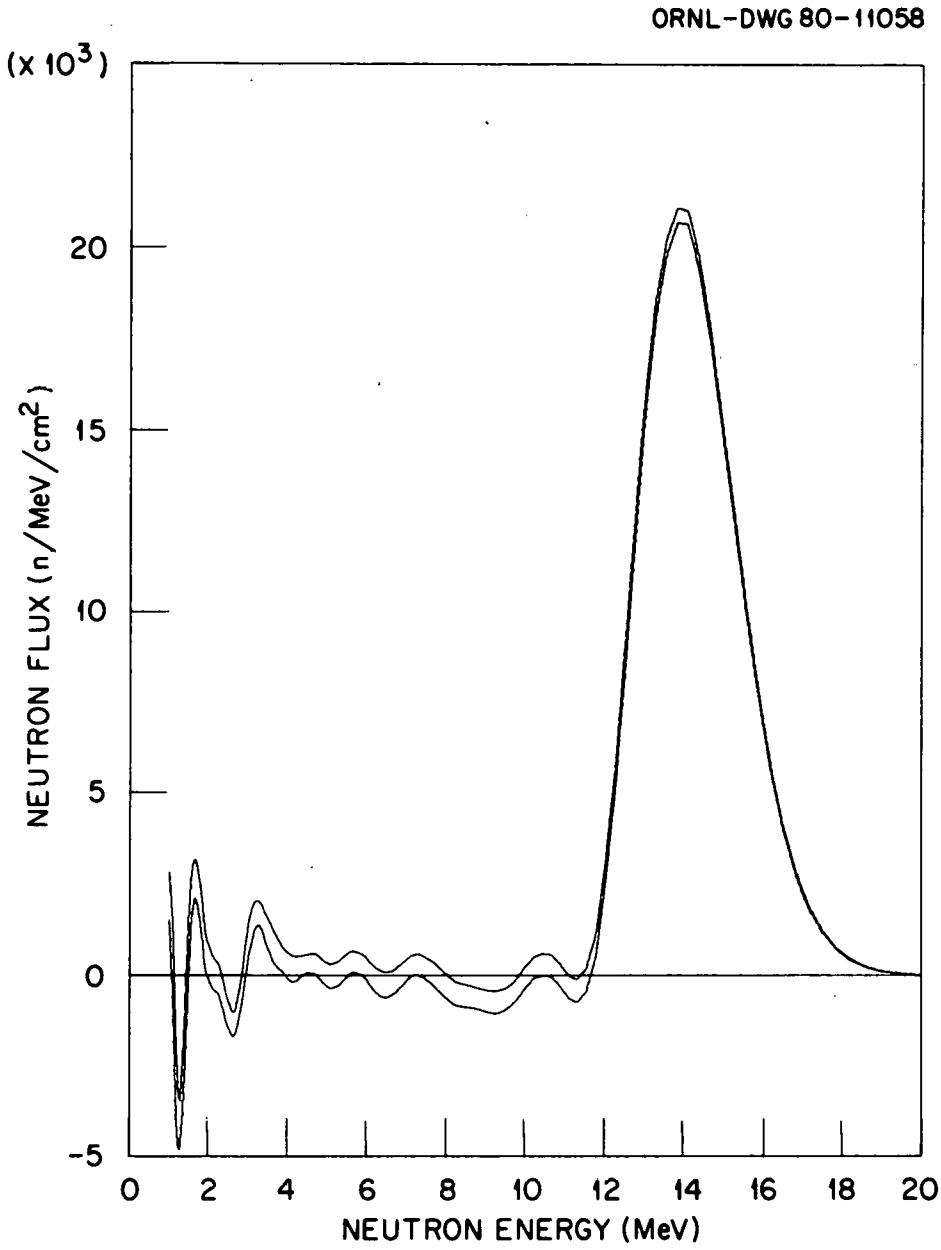

Fig. 2. NE-213 detector response to T(D,n) neutrons.

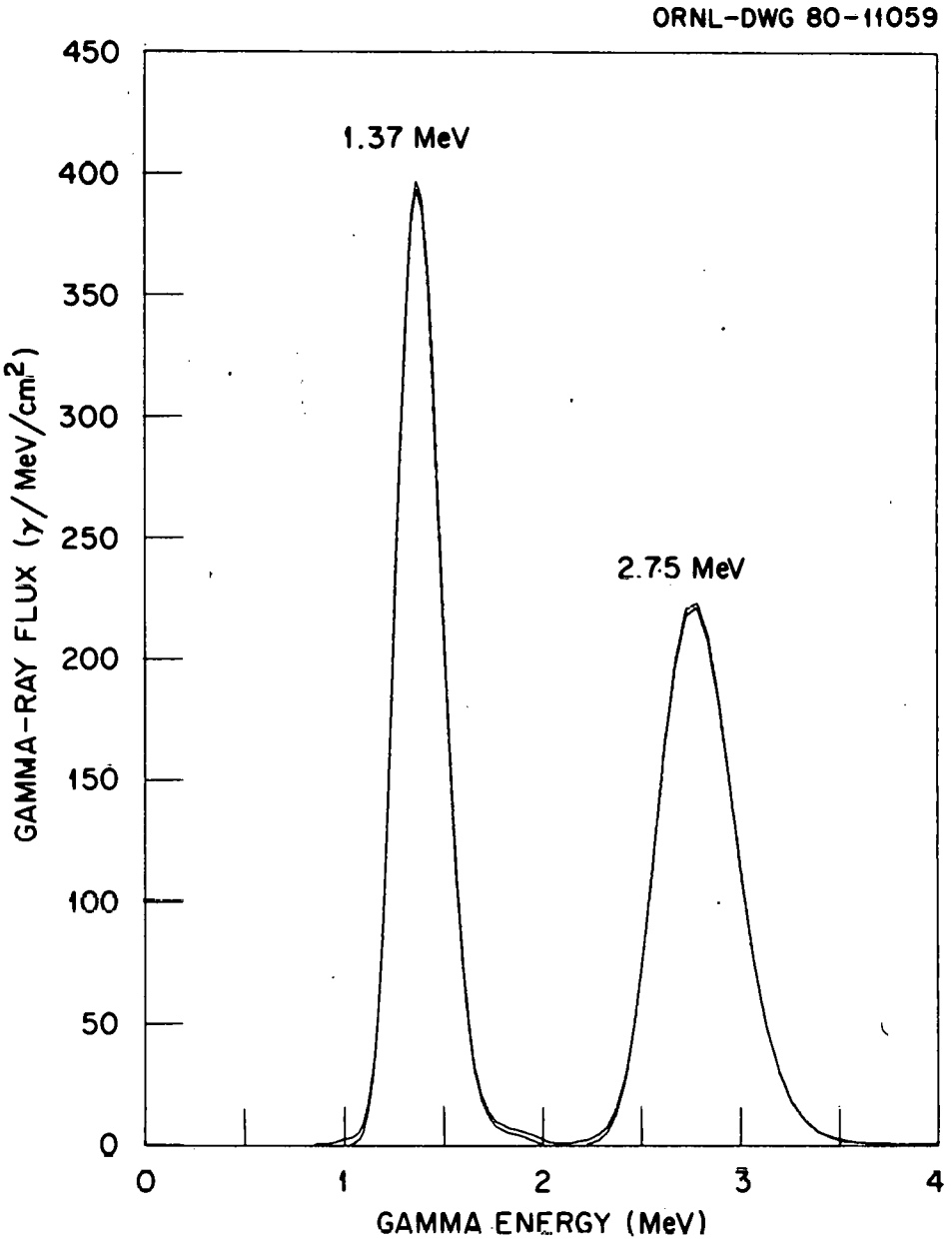

Fig. 3. NE-213 detector response to ^{24}Na gamma rays.

III. DETAILS OF THE CALCULATION

All of the calculated results were obtained using two-dimensional radiation transport methods. Figure 4 shows the calculational model used to approximate the experimental configuration. The concrete suppport structure, the test slabs, room and detectors were modeled in r-z geometry with cylindrical symmetry about the axis of deuteron injection. The components were modeled using 42 radial and 82 axial mesh intervals in a reduced geometry of the experimental room. That is, the walls and ceiling of the facility are replaced in the model by albedo surfaces at the axial and radial boundaries. An analysis was carried out to determine the validity of incorporating the albedo surfaces at these boundaries and the results of these studies may be found in Ref. 2. However, it was determined that a reflection factor of 20% for neutrons and gamma rays of all energies reproduced the scalar flux profiles in the vicinity of the detector locations in the reduced geometry compared to those obtained using a cylindrical representation of the full room. Compressing the geometry results in a smaller computer core size requirement and concommittant reduction in the transport code running time.

A typical test slab configuration is shown in the cavity in the concrete support structure in Fig. 4. Neutron and gamma ray energy spectra were measured and calculated as a function of the thickness and composition of the test slabs when the NE-213 scintillator detector was on the axis of symmetry and at a distance of 46 cm normal to the axis. In all cases, the source-to-detector axial distance was fixed at 154.5 cm. (The source-to-detector distance for the off axis detector location is 161.20 cm.)

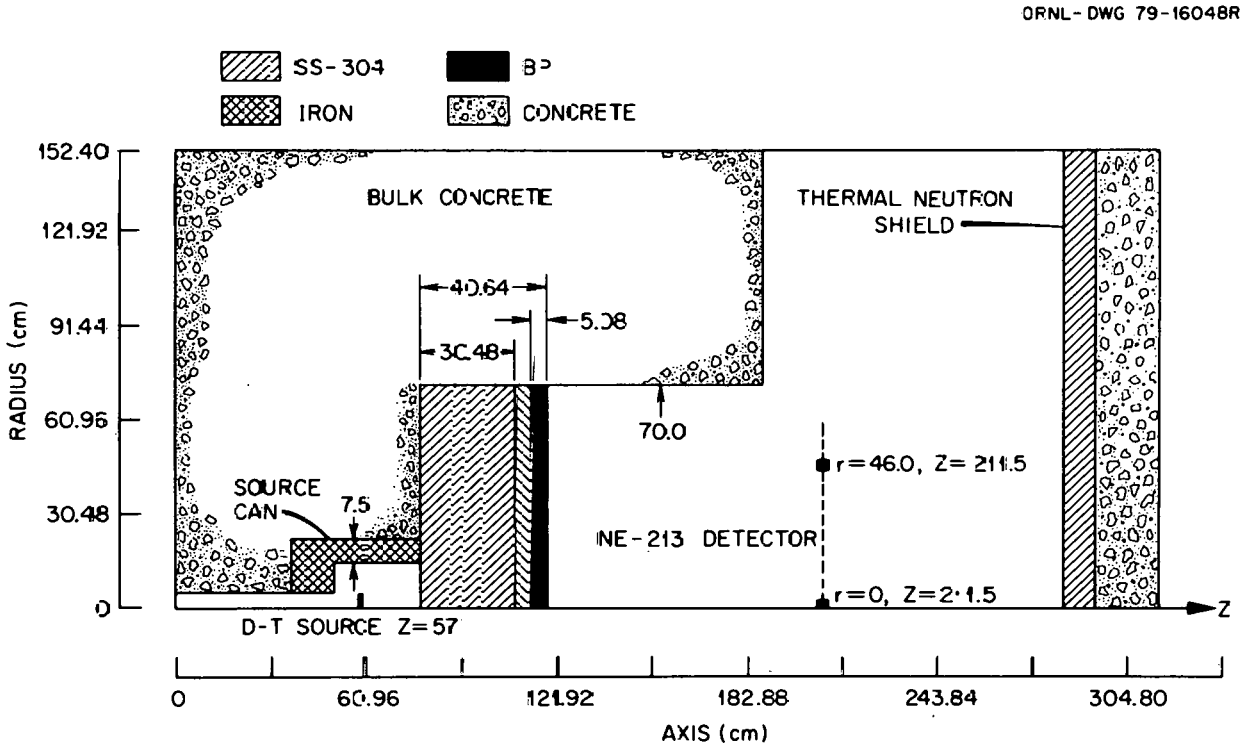

Fig. 4. Two-dimensicnal calculational model of the experimental configuration.

The sequence of radiation transport calculations to obtain the neutron and gamma ray spectra is complex and very detailed and is described fully in Ref. 2, so only the salient features are discussed here to facilitate the comparison of the measured and calculated neutron and gamma ray spectra.

The probability that a deuteron of energy E_d reacts while traveling a distance dx in a target containing N_t tritium atoms per cm^3 is

$$P = N_t \int_0^{E_d} \sigma dE/(dE/dx) \qquad (4)$$

where σ is the microscopic cross section for the T(D,n) ^{4}He reaction and dE/dx is the stopping power for deuterons in the target material. If σ is expressed as the angular differential cross section for the reaction, then P is also the probability for the emission of the neutron into any solid angle. Equation (4) can be used to determine the neutron emission probabilities for all deuteron energies and for all angles into which the neutron is emitted. The energies of the neutrons are then obtained as a function of E_d and emission angle using the kinematic equations for a two-body reaction. The probabilities for the emission of neutrons into the angular intervals of 0-40, 40-90, and 90-180 degrees with respect to the axis of deuteron injection from the reactions of 250 keV deuterons in a 4 mg/cm^2 thick titanium-tritide target are given as a function of neutron energy in Table I.* The energy dependence of the neutrons from the D-T reaction varies by ∿14% between 0 and 180 degrees. The anglar interval of 0-40 degrees corresponds to the angle at which neutrons are emitted

*The energy intervals correspond to the energy boundaries of the group structure used to describe the multigroup cross sections.

directly out of the mouth of the can. (The polar angle defined by a ray from the D-T source to the mouth of the can is ∿40 degrees.) The 40-90 and 90-180 degree angular intervals correspond to the angles at which neutrons are emitted into the lateral surface and towards the rear of the can, respectively. These angular intervals were selected on the basis of the source can geometry. A finer angular mesh could have been adopted with no affect on the final results, but at the expense of additional computing time. These data serve as the input to the radiation transport codes used to calculate the neutron and gamma ray energy spectra.

Table I

Angle-Energy Dependence for Neutrons Emitted From the T(D,n) ^{4}He Reaction (E_d = 250 keV)

Energy Interval (MeV)		Angular Interval		
		0°-40°	40°-90°	90°-180°
14.92	15.68	0.0130		
14.55	14.92	0.0902	0.0697	
14.19	14.55	0.0168	0.2460	
13.80	14.19		0.0750	0.2163
13.50	13.80			0.2088
12.84	13.50			0.0642
		0.1200	0.3907	0.4893

All of the radiation transport calculations used to obtain the data reported here incorporated a 53-neutron, 21-gamma-ray energy group library obtained by collapsing the 171-neutron, 36-gamma ray VITAMIN C data library (ENDF/B-IV).[5] The VITAMIN C library was created as a general purpose cross section data set for the analysis of fusion neutronics problems. The fine group library was collapsed using the ANISN[6] code by representing the experimental components in the angular intervals given in Table I in spherical geometry and using the neutron angle energy distribution in that angular interval as the energy weighting function. The energy boundaries of the collapsed data library, given in Table II, were based in part on those used in the DLC-47 library[7], but expanded at high energies so that the D-T neutron source could be more accurately represented in the transport calculations. The angular dependence of the cross sections for all nuclei was approximated using a P_3 Legendre expansion. The composition of the materials used in the calculations is given in Table III.

The sequence of radiation transport calculations used to obtain the neutron and gamma ray energy spectra is shown in Fig. 5. The sequence is initiated by performing three separate calculations using the GRTUNCL code [8] to obtain the uncollided neutron and first collision source distributions at all spatial mesh intervals in the calculational geometry. The purpose for performing these calculations separately is to account for the angle-energy dependence of the D-T neutron source. To insure that the contributions to the uncollided neutron flux and first collision sources were due to neutrons emitted into the angular intervals specified in Table I, black absorbers were interposed in the calculational geometry to confine the source neutrons to those angles. Also, the GRTUNCL code assumes

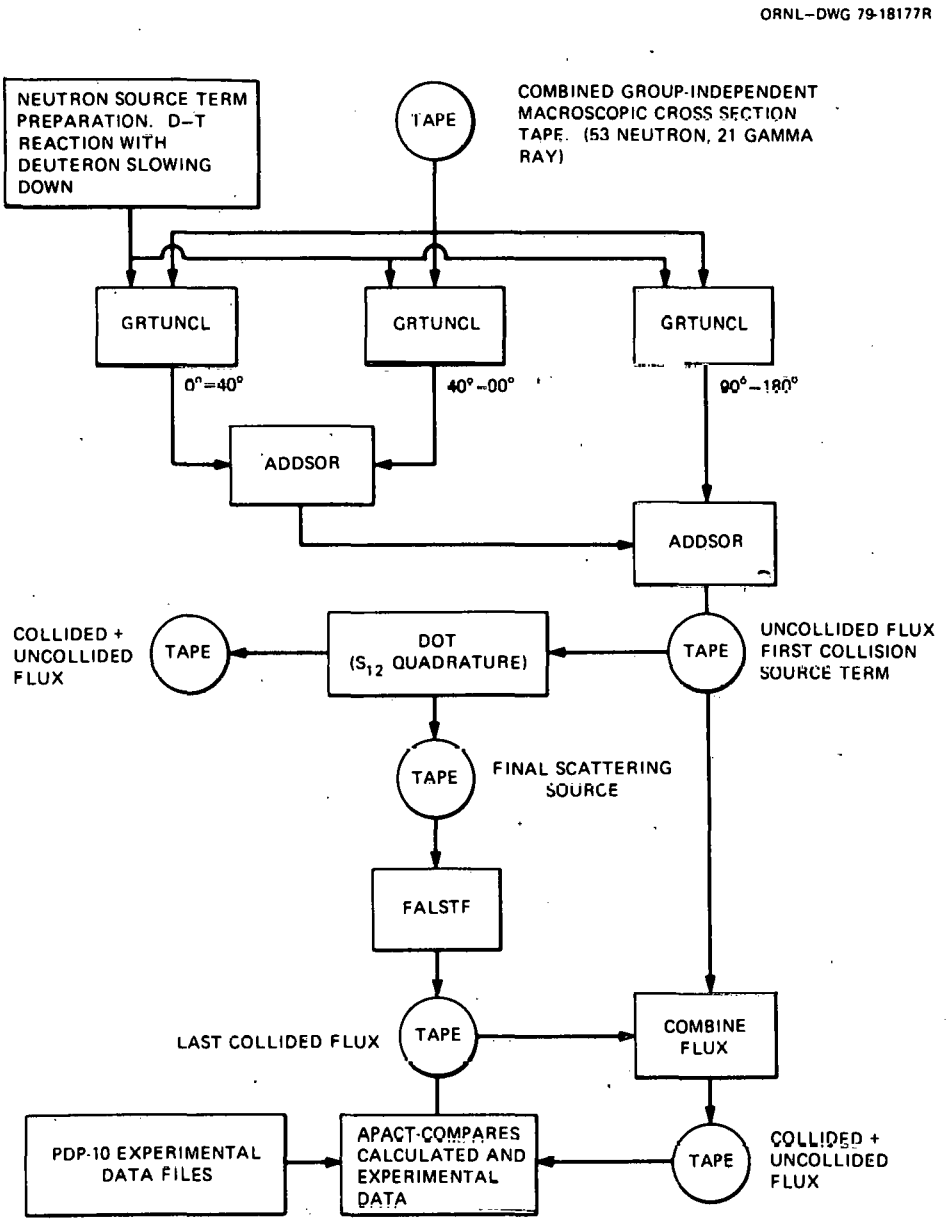

Fig. 5. Sequence of calculations to obtain neutron and gamma ray energy spectra.

Table II. 53-Neutron, 21-Gamma-Ray Energy Radiation Transport Cross Section Group Structure

Neutron Group	Upper Energy (eV)	Neutron Group	Upper Energy (eV)	Gamma Ray Group		Upper Energy (MeV)
1	0.17333E + 08	28	0.60810E + 06	54	1	14.0
2	0.15683E + 08	29	0.49787E + 06	55	2	12.0
3	0.14918E + 08	30	0.36883E + 06	56	3	10.0
4	0.14550E + 08	31	0.29850E + 06	57	4	8.0
5	0.14191E + 08	32	0.29720E + 06	58	5	7.5
6	0.13840E + 08	33	0.18316E + 06	59	6	7.0
7	0.13499E + 08	34	0.11109E + 06	60	7	6.5
8	0.12840E + 08	35	0.67379E + 05	61	8	6.0
9	0.12214E + 08	36	0.40868E + 05	62	9	5.5
10	0.11052E + 08	37	0.24788E + 05	63	10	5.0
11	0.10000E + 08	38	0.23579E + 05	64	11	4.5
12	0.90484E + 07	39	0.15034E + 05	65	12	4.0
13	0.81873E + 07	40	0.91188E + 04	66	13	3.5
14	0.74082E + 07	41	0.55308E + 04	67	14	3.0
15	0.60653E + 07	42	0.33546E + 04	68	15	2.5
16	0.49659E + 07	43	0.20347E + 04	69	16	2.0
17	0.40657E + 07	44	0.12341E + 04	70	17	1.50
18	0.36788E + 07	45	0.74852E + 03	71	18	1.0
19	0.27253E + 07	46	0.45400E + 03	72	19	0.60
20	0.23653E + 07	47	0.27536E + 03	73	20	0.20
21	0.23069E + 07	48	0.16702E + 03	74	21	0.10
22	0.22313E + 07	49	0.10130E + 03			0.010
23	0.16530E + 07	50	0.61442E + 02			
24	0.13534E + 07	51	0.37267E + 02			
25	0.86294E + 06	52	0.10077E + 02			
26	0.82085E + 06	53	0.41399E + 00			
27	0.74274E + 06		0.10000E - 04			

Table III. Composition of Materials Used in the Calculation

	Composition (atom/cm-Barn)					
Element	Concrete	Air	Iron Can	SS-304	BP*	Hevimet
H	7.86×10^{-3}				7.13×10^{-2}	
B-10					4.87×10^{-4}	
B-11					1.97×10^{-3}	
C					3.41×10^{-2}	
N		3.64×10^{-5}				
O	4.39×10^{-2}	9.74×10^{-6}			3.64×10^{-3}	
Na	1.05×10^{-3}					
Mg	1.40×10^{-4}					
Al	2.39×10^{-3}					
Si	1.58×10^{-2}					
K	6.90×10^{-4}					
Ca	2.92×10^{-3}					
Cr				1.77×10^{-2}		
Mn				1.77×10^{-3}		
Fe	3.10×10^{-4}		8.48×10^{-2}	6.02×10^{-2}		
Ni				7.83×10^{-3}		1.05×10^{-2}
Cu						6.45×10^{-3}
W-182						1.32×10^{-3}
W-183						7.21×10^{-3}
W-184						1.54×10^{-2}
W-186						1.43×10^{-2}

*BP = Borated Polyethylene

isotropic neutron emission from a point source. To account for the anisotropy of the D-T neutrons the neutron angle-energy probabilities, $P(\Delta E,\Delta\Theta)$, from Table I were weighted using a solid angle factor given by

$$P_W(\Delta E,\Delta\Theta) = \frac{2P(\Delta E,\Delta\Theta)}{\int_{\Theta_1}^{\Theta_2} \sin\Theta' d\Theta'} \tag{5}$$

where $P_W(\Delta E,\Delta\Theta)$ is the solid angle weighted probability for neutrons in the energy interval ΔE emitted into the angular interval $\Delta\Theta$ and Θ is measured relative to the deuteron-target axis.

The first collision source data from each GRTUNCL calculation is combined to form a single source which is the input data to the two-dimensional discrete ordinates code DOT.[9] This code calculates the collided flux distributions using the first collision data as a spatially distributed source. These calculations were completed using an S_{12} angular quadrature. A final scattering source tape is generated in DOT and is employed to carry out a last-flight transport calculation using the FALSTF code[8] to obtain the neutron and gamma ray energy dependent flux at each detector location. The output from FALSTF is combined with the uncollided flux data from GRTUNCL to yield the total flux at each detector location. These total fluxes are processed to obtain the neutron and gamma ray energy spectra by smoothing the flux per unit energy in each multigroup energy interval with an energy-dependent Gaussian response function having a width determined by Eq. (2) for neutrons, and Eq.(3) for gamma rays. Performing the calculations in the sequence shown in Fig. 5 assures that ray effects from the DT neutron source, as well as

those from intense last collision sources from neutron reactions with experimental components are eliminated.

III. DISCUSSION OF RESULTS

Neutron and gamma ray energy spectra have been measured and calculated as a function of detector position behind laminated slabs of stainless steel type-304 (SS-304) and borated polyethylene (BP) having compositions and thicknesses as shown in Table IV. In configurations 1-3, the SS-304 thickness varied between 0 to 30.48 cm in steps of 15.24 cm. Thereafter, the total shield thickness was increased by the addition of 5.08-cm-thick slabs of SS-304 and BP, in various combinations, to a maximum thickness of 55.88 cm. The composition and thickness of the laminated slabs were selected on the basis of being representative of the stainless steel plus hydrogeneous material combinations that may be used in fusion reactor shields. The incorporation of thick stainless steel layers immediately behind the neutron source slow down the 14-MeV neutrons to energies where the hydrogeneous material layers are effective in moderating the neutrons. Borated polyethylene was selected as the hydrogeneous material because it was readily available (in the appropriate thickness and cross sectional dimensions for use in the experiment) and because, from the point of view of both the measurements and analysis, it would serve the same purpose neutronically as other candidate shield materials such as borated water or boron carbide.

The measured and calculated differential neutron energy spectra as a function of SS-304 and BP slab composition and thickness are compared in Fig. 6 when the NE-213 detector is on the axis of symmetry. The neutron source-to-detector distance is 154.5 cm. In Fig. 6, and the

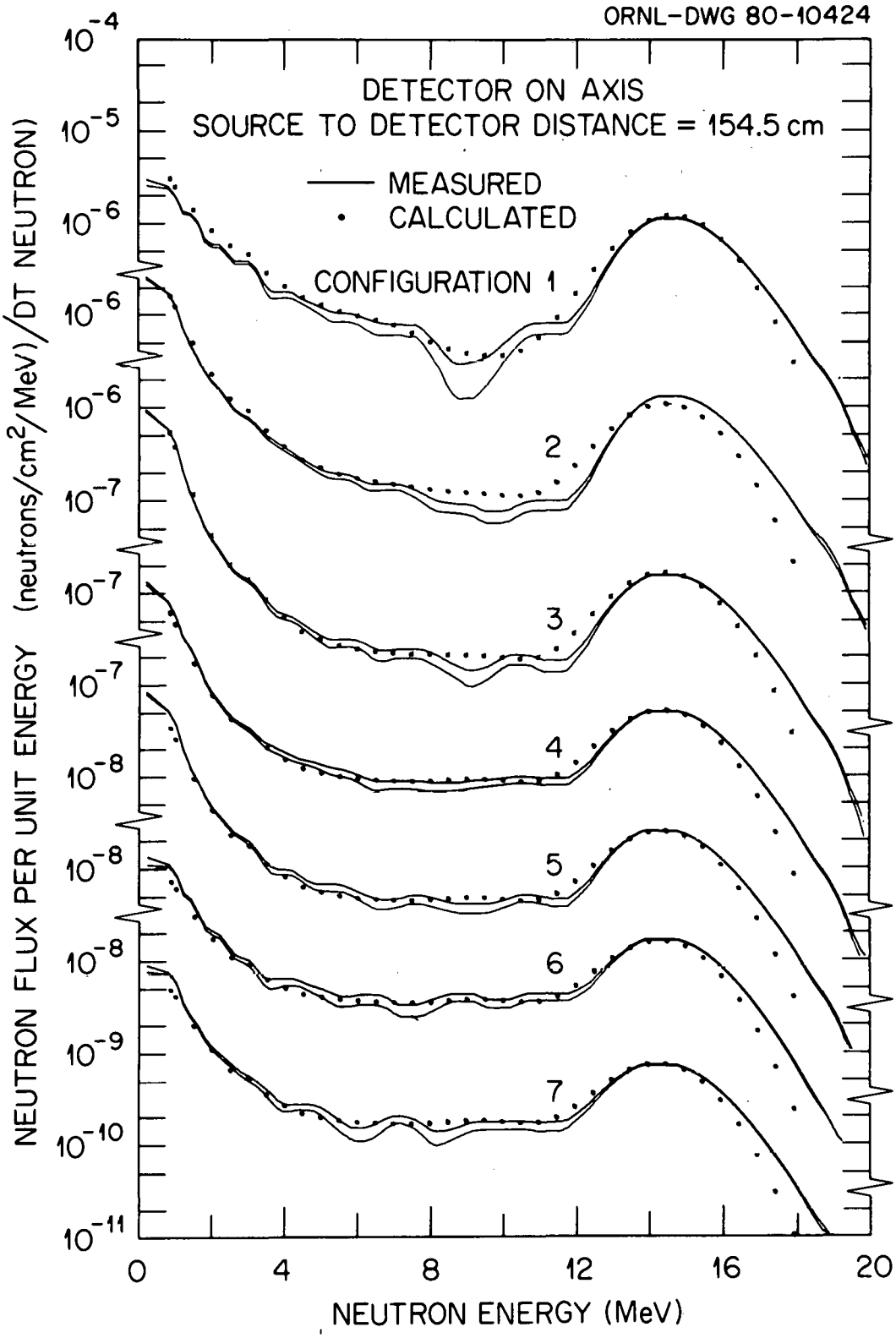

Fig. 6. Neutron flux per unit energy vs. neutron energy as a function of SS-304 and BP slab composition and thickness for the detector on axis. (Note breaks in ordinate)

Table IV. Composition and Thickness of Stainless Steel 304 and Borated Polyethylene Slabs

Configuration	Composition						Total Slab Thickness (cm)
	SS-304[a]	SS-304	BP[b]	SS-304	BP	SS-304	
	Slab Thickness (cm)						
1	0						0
2	15.24						15.24
3	30.48						30.48
4	30.48	5.08	5.08				40.64
5	30.48	5.08	5.08	5.08			45.72
6	30.48	5.08	5.08	5.08	5.08		50.80
7	30.48	5.08	5.08	5.08	5.08	5.08	55.88

[a]Stainless steel type 304

[b]Borated polyethylene

comparisons of other data given below, the solid curves are measured spectra and the points are the calculated results. The two solid curves for each configuration represent one standard deviation in the measured spectra and is introduced by the unfolding procedure to obtain energy spectra from the pulse height data. The spectra are arranged in order of increasing slab thickness from top-to-bottom in the figure and both the measured and calculated data are normalized to one D-T neutron.

The spectra are compared for neutron energies above 850 keV. The calculated and measured spectra are in excellent agreement for all of the configurations except when the slab contains 15.24 cm of SS-304 (configuration 2).

In all of the spectra, however, the agreement is favorable in the neutron energy range between 850 keV and ∿11 MeV. The calculated results are systematically higher than the measured data between ∿11 and 12.5 MeV, in good agreement between 12.5 and ∿15 MeV and then the calculated data exhibit a more rapid roll-off at the higher neutron energies.

It is not kinematically possible for the incident deuterons (250 keV) to produce neutrons with energies above 15.1 MeV in the D-T reaction. The indication of more energetic neutrons in the spectra is a manifestation of the response of the experimental instrumentation and the difference in the roll-off at neutron energies above ∿15 MeV can be attributed to the Gaussian response function being convoluted with neutron energy bins (pulse height channels and multigroup energy intervals) that differ between measured and calculated data.

The integrated neutron energy spectra, obtained by integrating the distributions in Fig. 6, are compared in Fig. 7. The measured and calculated data are in excellent agreement for all of the slab configurations except for that comprised of 15.24 cm of SS-304 (configuration 2). The data agree within ∿5% for neutron energies between 850 keV and ∿15 MeV. At the higher neutron energies, the measured and calculated data exhibit larger differences, but these can be attributed to the Gaussian smoothing phenomena as noted above.

The measured and calculated differential and integral neutron energy spectra as a function of SS-304 and BP slab composition and thickness when the detector is off the axis of symmetry are compared in Figs. 8 and 9, respectively. The NE-213 detector was positioned at a distance of 46.0 cm normal to the deuteron beam - tritium target axis for all of the slab configurations except for that comprised of 30.48 cm of SS-304 (configuration 3). For this measurement, the detector was located at a distance of 100 cm from the beam axis. A series of measurements of neutron spectra in the plane perpendicular to the deuteron beam axis revealed that the neutron yield was symmetric about the axis. Consequently, the incorporation of the two-dimensional representation of the experimental apparatus and the detector location in the r-z geometry of the calculational model can be correlated with the actual detector location in the cartesian coordinate system of the experiment.

The measured and calculated data are compared for slab configurations 2-7. The data compare favorably for all of the cases except for the slab configuration comprised of 30.48 cm of SS-304 (configuration 3). The neutron flux distributions in the reduced geometry of the calculational

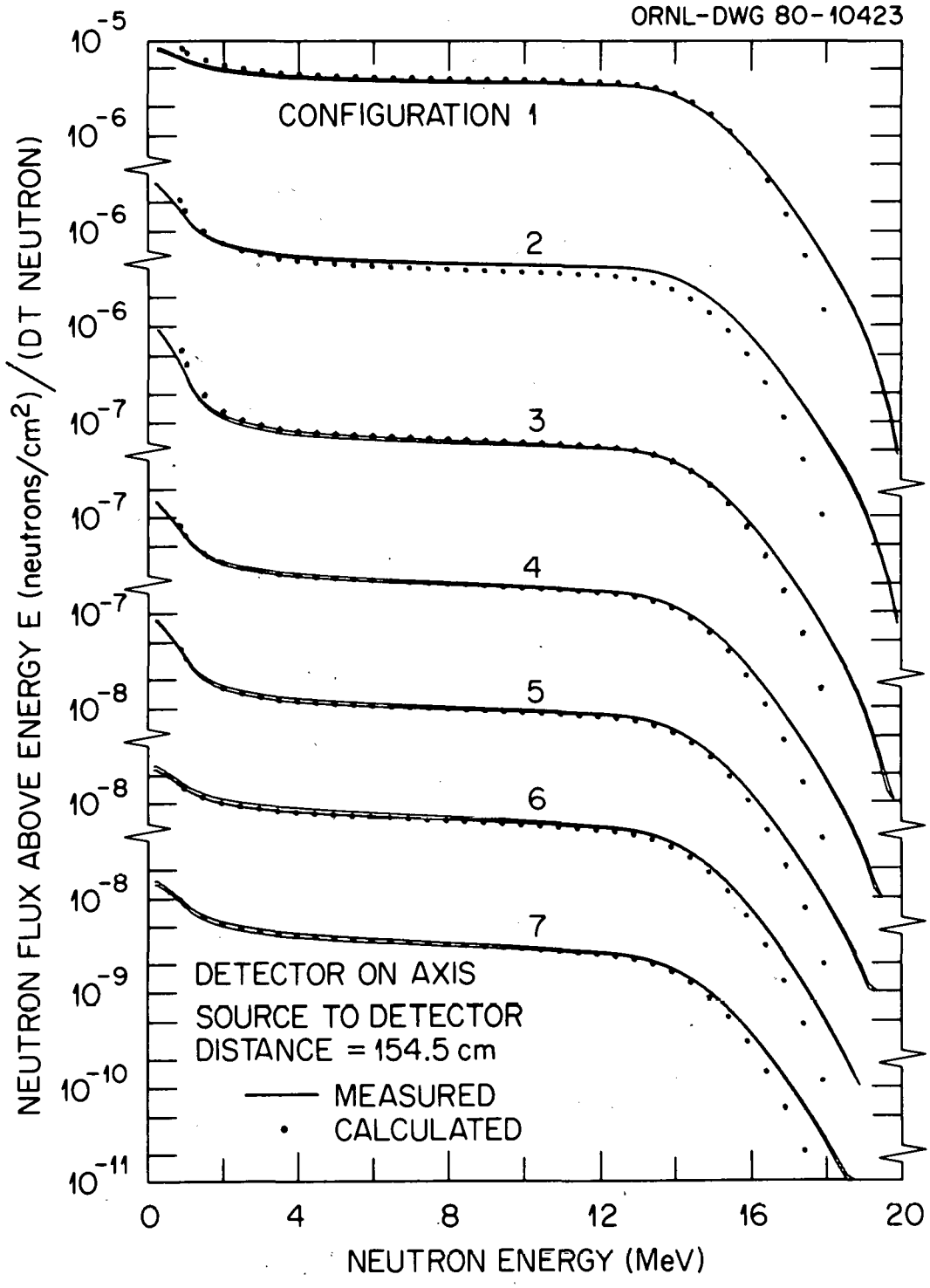

Fig. 7. Neutron flux above energy E vs. neutron energy as a function of SS-304 and BP slab composition and thickness for the detector on axis. (Note breaks in the ordinate)

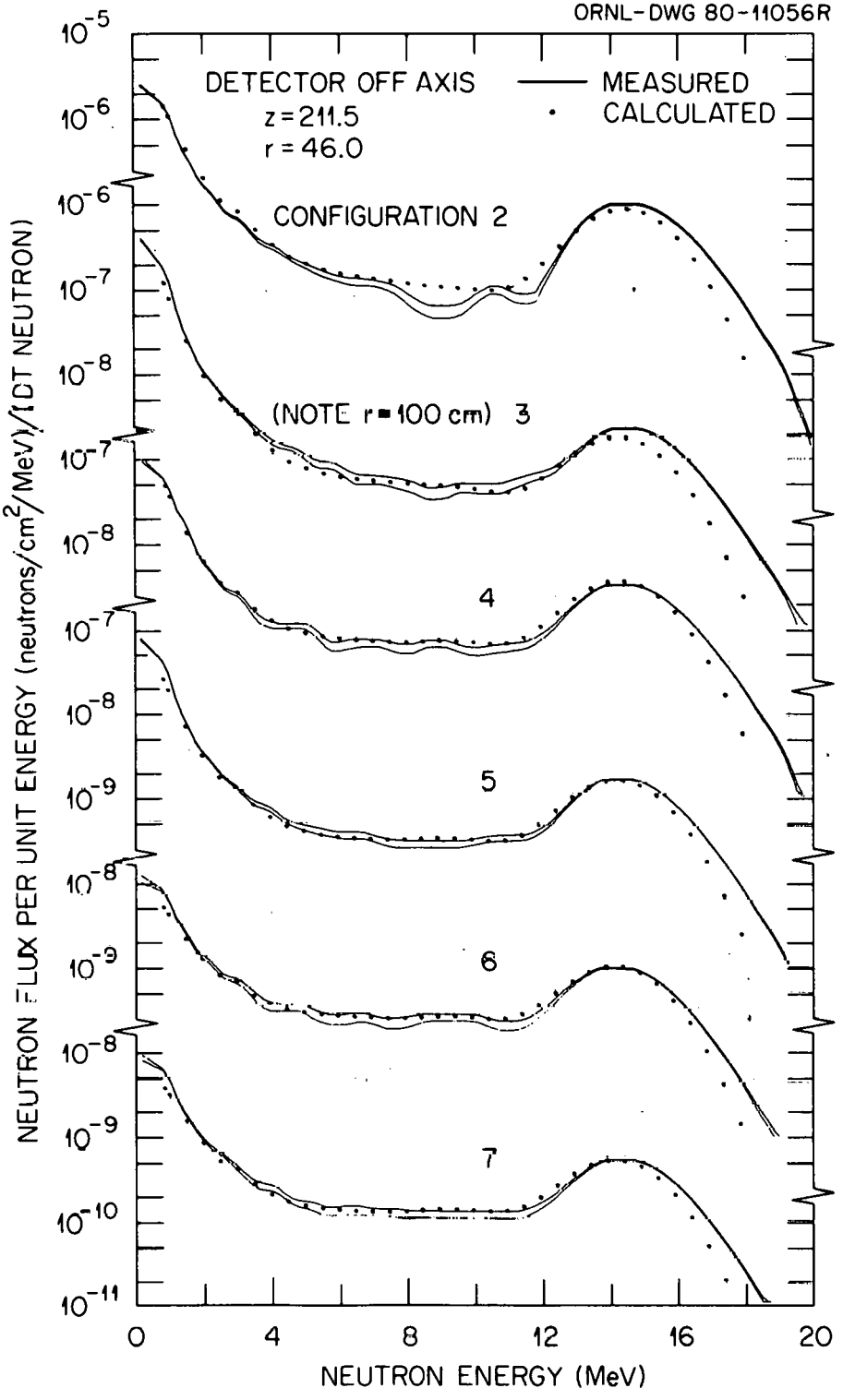

Fig. 8. Neutron flux per unit energy vs. neutron energy as a function of SS-304 and BP slab composition and thickness for the detector off axis. (Note breaks in the ordinate)

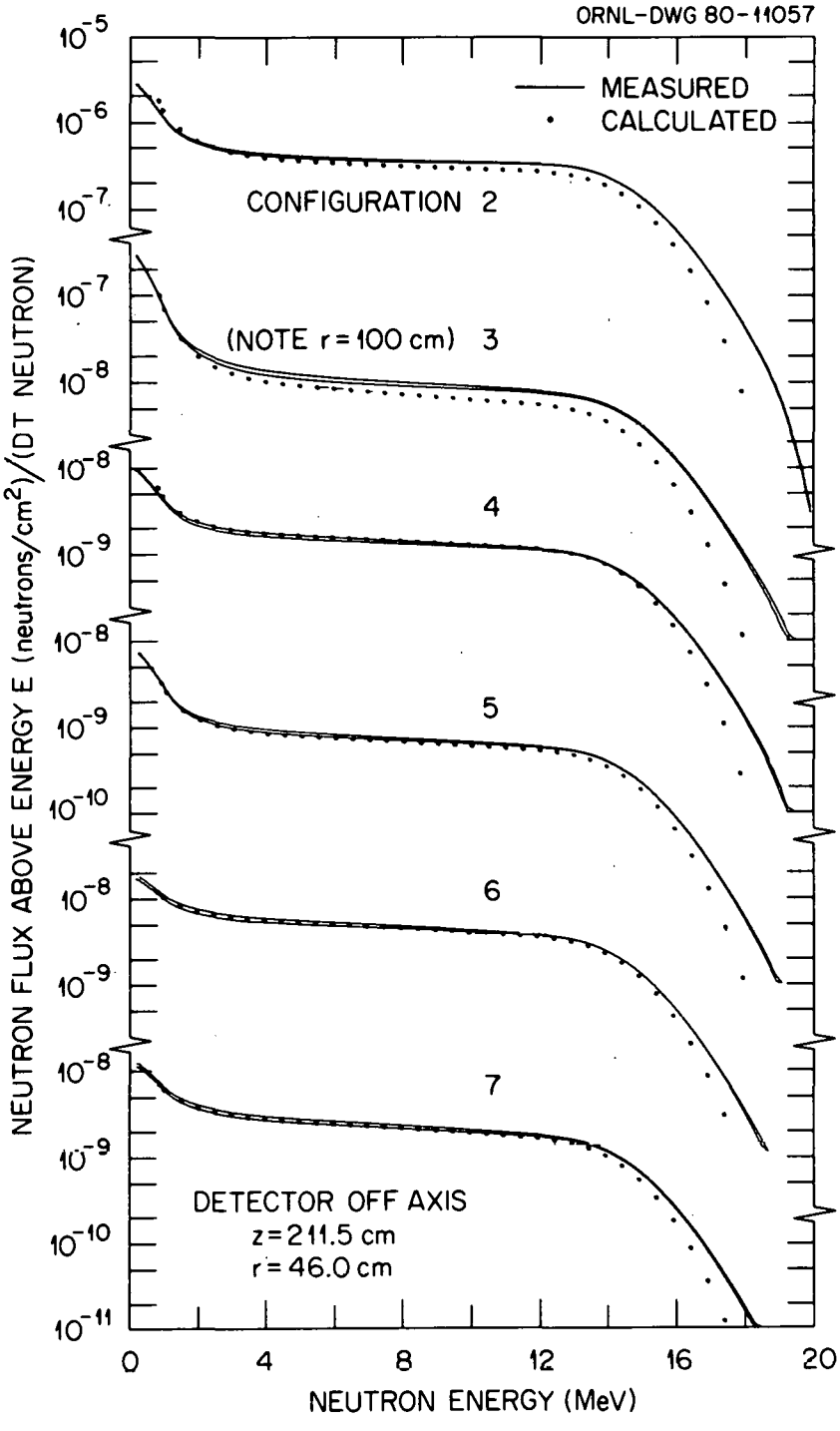

Fig. 9. Neutron flux above energy E vs. neutron energy as a function of SS-304 and BP slab composition and thickness for the detector off axis. (Note breaks in the ordinate)

model are not reproduced to the same precision as those obtained in the full room geometry at 100 cm from the axis as they are at 46.0 cm from the axis.[2] For this case, a different neutron reflection factor may be required at the albedo surfaces in the calculational model to reproduce the measured results.

The differential and integral gamma ray energy spectra for the cases with the detector on and off the axis of symmetry as a function of SS-304 and BP slab thickness and composition are compared in Figs. 10-13. The measured and calculated spectra are compared for gamma rays having energies above 750 keV. The measured and calculated data are in good agreement for gamma rays with energies to ∿8 MeV. The calculation reproduces the measurements in magnitude but because of the rather coarse energy group structure, the various peaks in the measured differential distributions are not reproduced. The important point to note in these comparisons is that the gamma rays that contribute to these spectra are due, in large part, to the reactions of low energy neutrons (<850 keV) with the slab materials. Although the neutron spectra are compared for energies greater than 850 keV, the radiation transport calculation was completed for neutrons down to thermal energies. Correspondingly, some of the gamma rays appearing in the distributions in Figs. 10-13 are due to thermal neutron capture reactions and these photons are accounted for in the calculation.

The calculations to determine the neutron and gamma ray energy spectra for the slab configuration containing the tungsten alloy, Hevimet, were carried out using the model of the experimental geometry shown in Fig. 14. The slab configuration consisted of layers of SS-304 and BP in the same order and thickness as configuration 5 (see Table IV) but with the addition

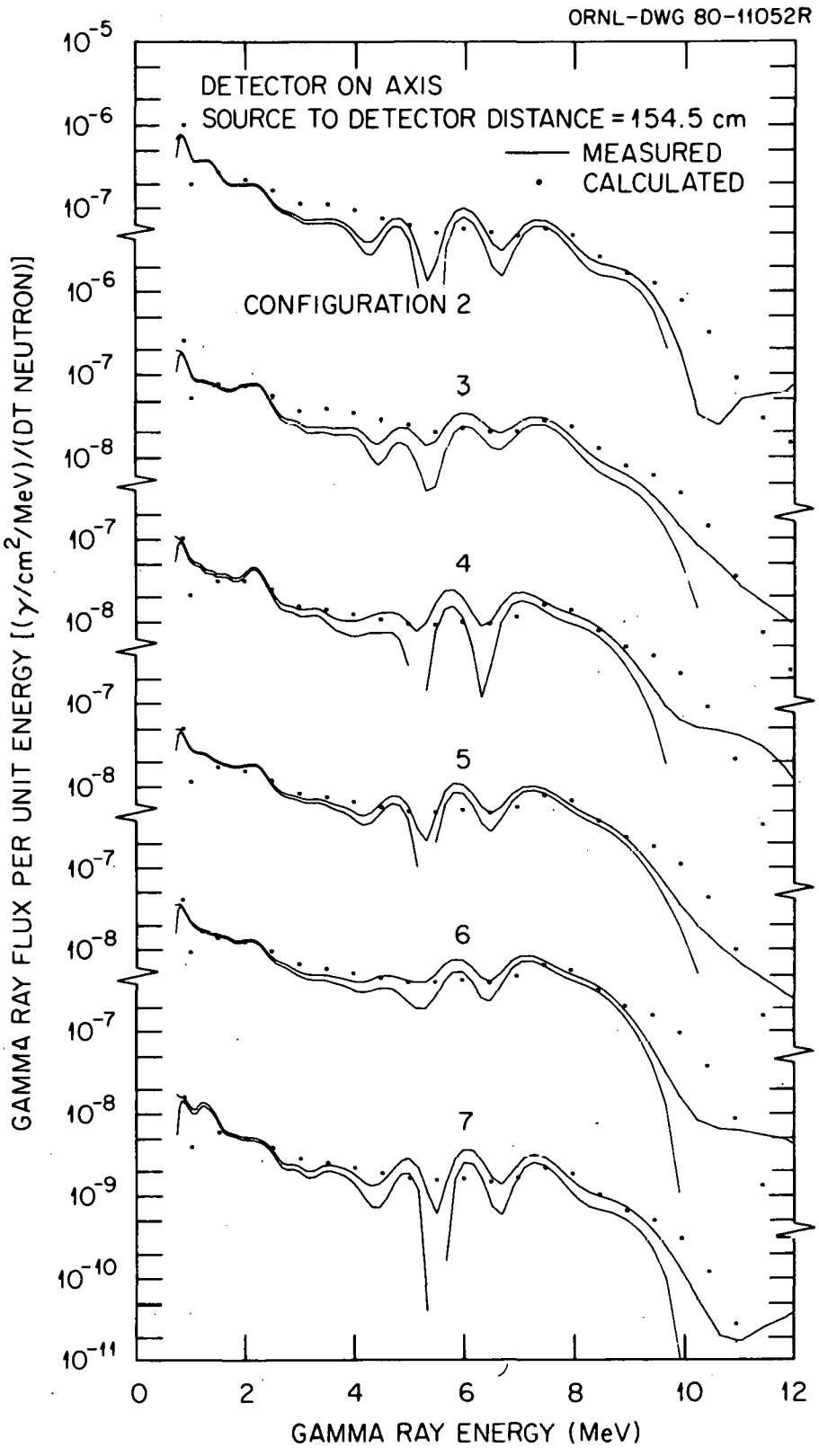

Fig. 10. Gamma ray flux per unit energy vs. gamma ray energy as a function of SS-304 and BP slab composition and thickness for the detector on axis. (Note breaks in the ordinate)

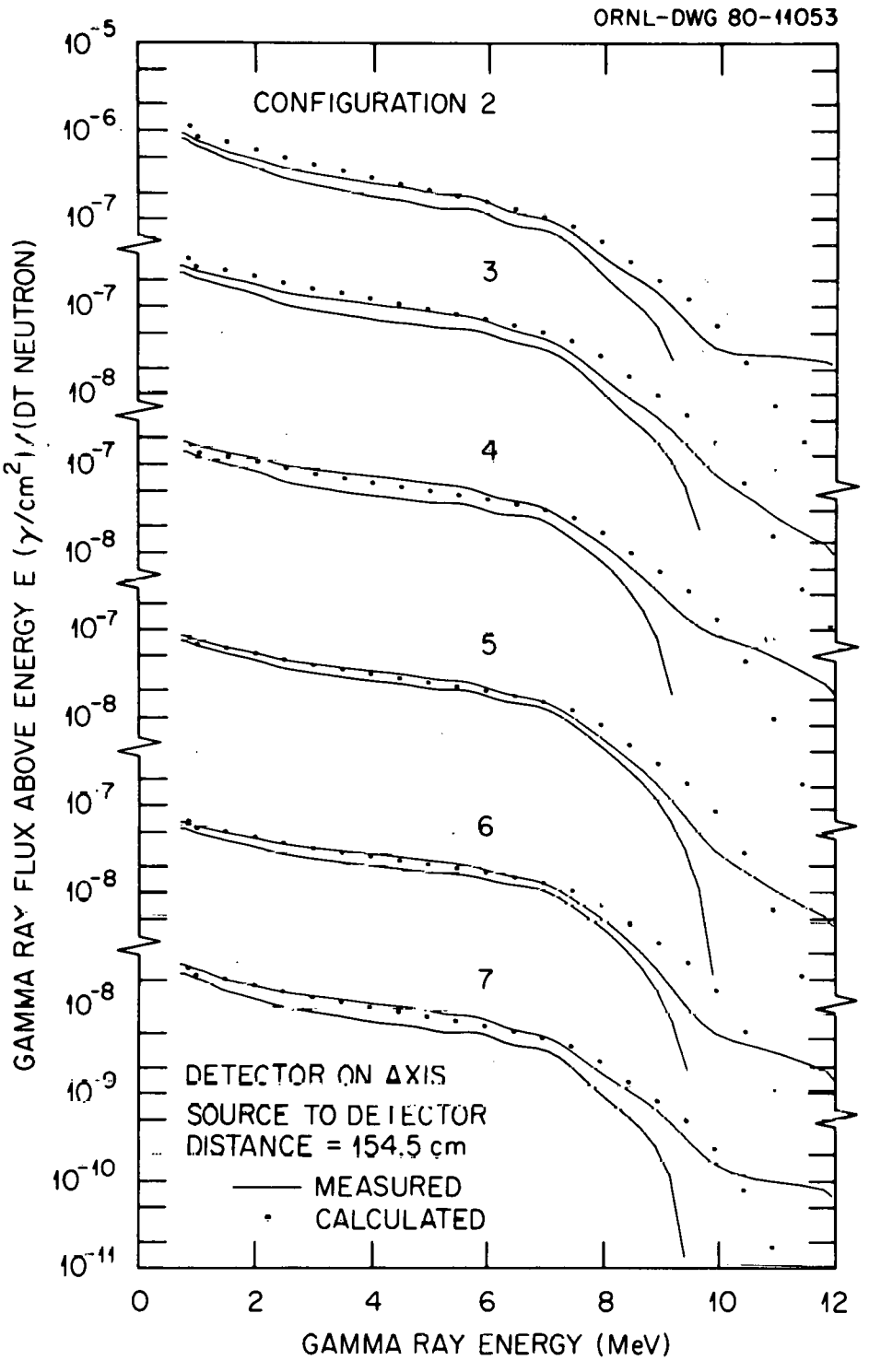

Fig. 11. Gamma ray flux above energy E vs. gamma ray energy as a function of SS-304 and BP slab composition and thickness for the detector on axis. (Note breaks in the ordinate)

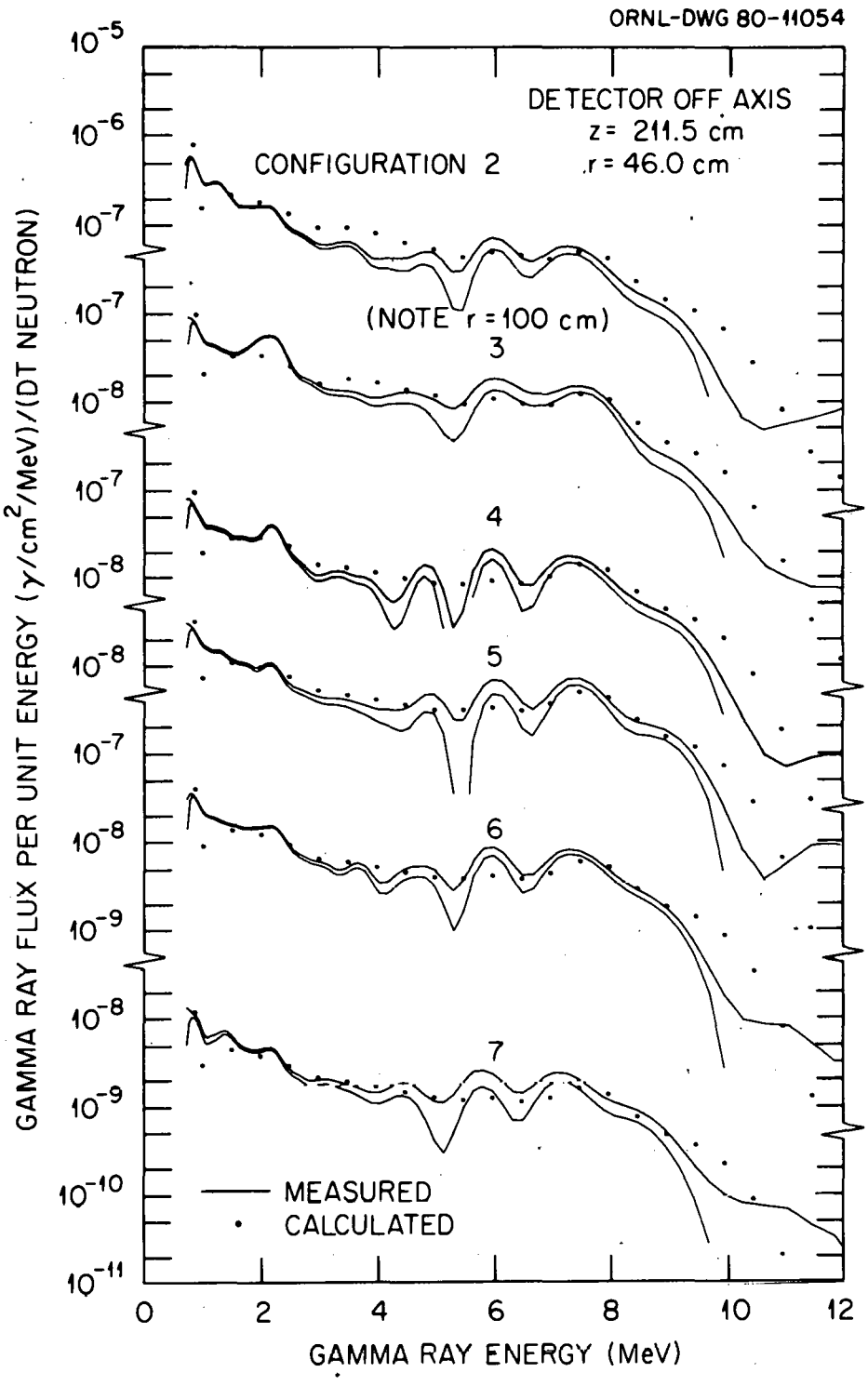

Fig. 12. Gamma ray flux per unit energy vs. gamma ray energy as a function of SS-304 and BP slab composition and thickness for the detector off axis. (note breaks in the ordinate)

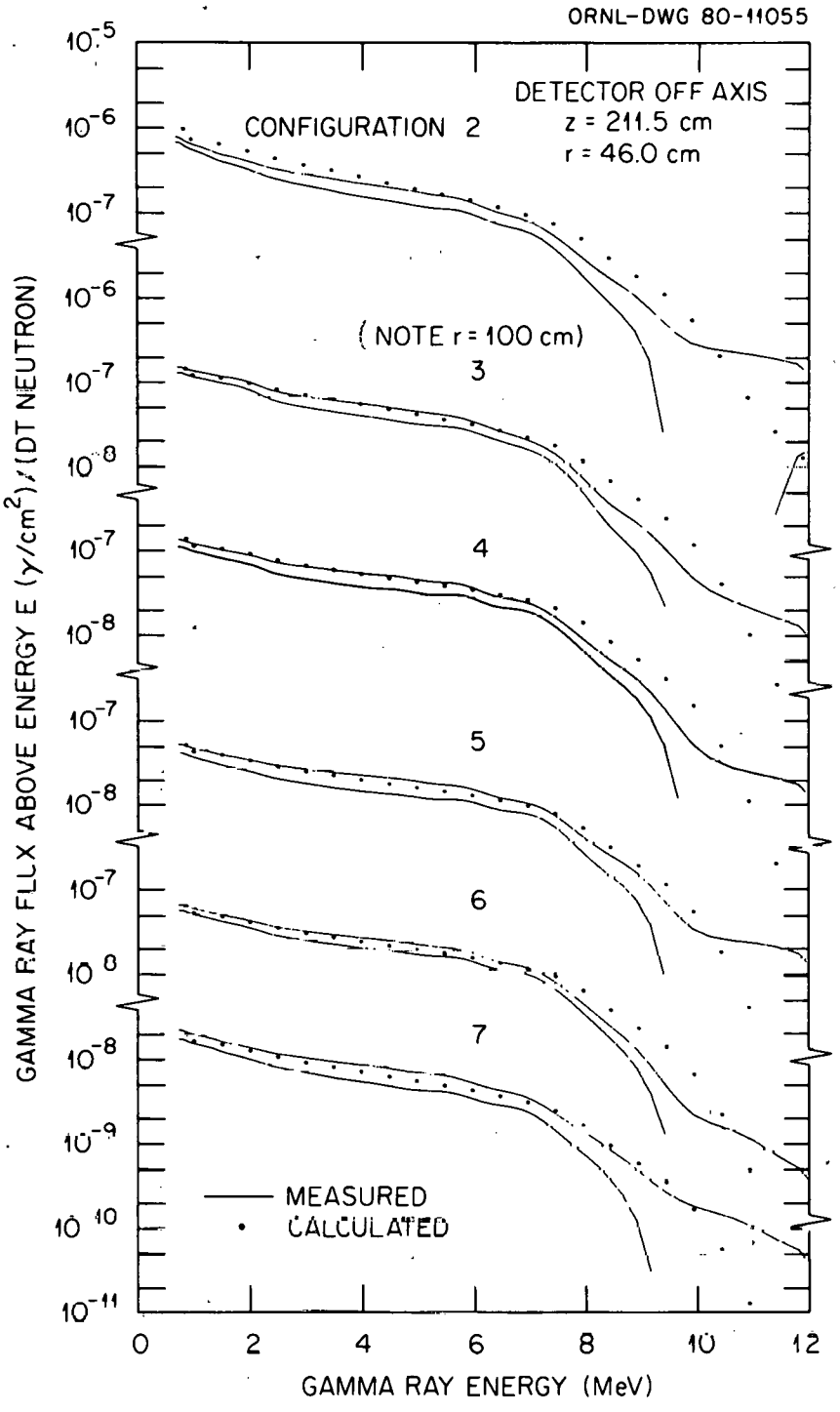

Fig. 13. Gamma ray flux above energy E vs. gamma ray energy as a function of SS-304 and BP slab composition and thickness for the detector off axis. (note breaks in the ordinate)

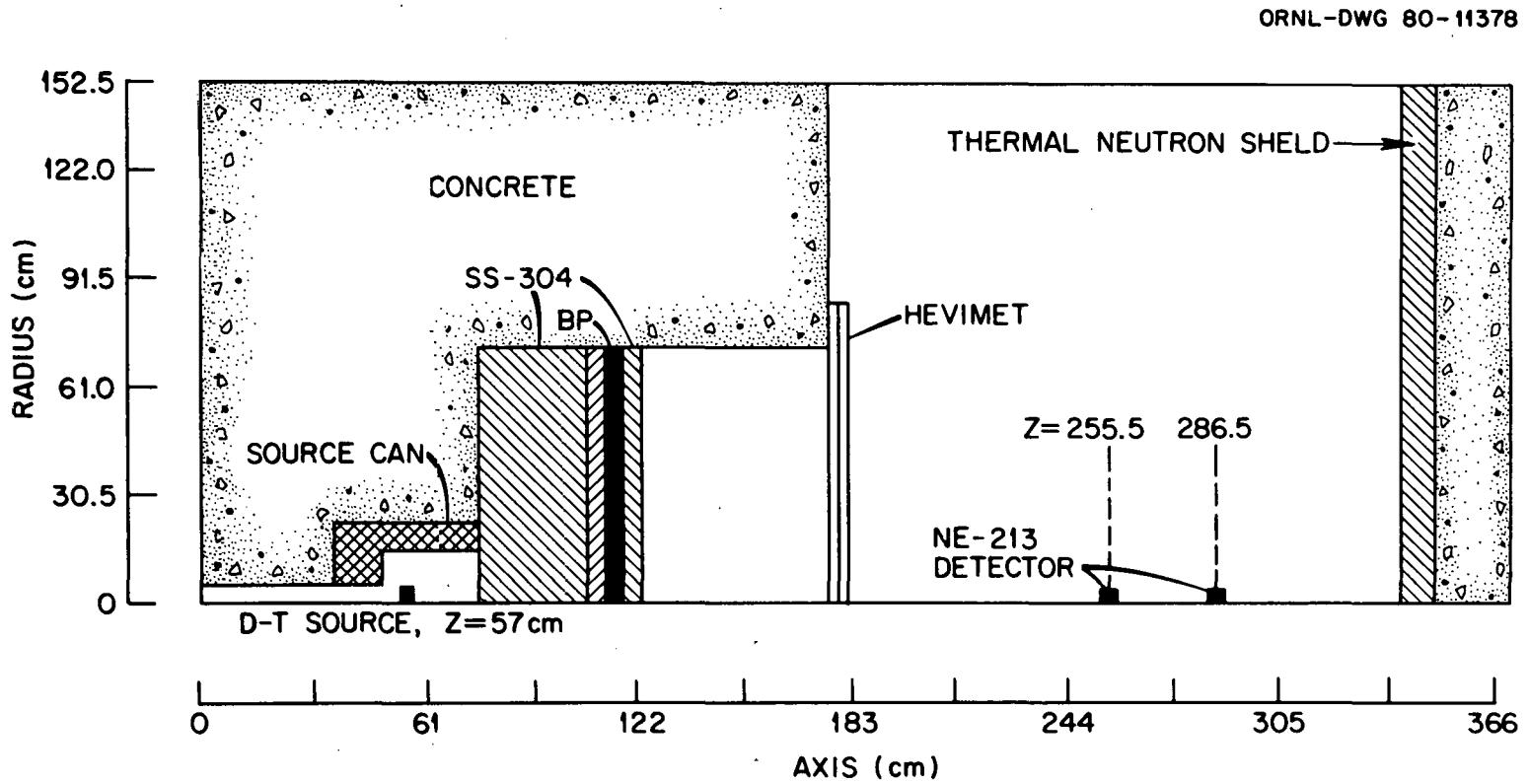

Fig. 14. Two-dimensional calculational model of the experimental configuration including hevimet as a slab material.

of 5.08 cm of Hevimet as the last layer. However, the Hevimet slab had lateral dimensions that were larger than the SS-304 or BP which prevented its insertion in the cavity in the concrete support structure, so this slab was mounted on the face of the concrete across the mouth of the opening. The axial dimension of the calculational model was also increased compared to that in Fig. 4 since the measurements were made with the detector at distances from the target of 198.5 and 229.5 cm. Both measurements were made with the detector on axis. The distance from the detector locations to the thermal neutron shield was maintained at ∿50 cm.

The measured and calculated neutron differential and integral energy spectra at the two detector locations are compared in Fig. 15. The differential spectra are compared in the upper portion of the figure and the integral spectra are compared in the lower portion of the figure. In both cases, the calculation reproduces the shape of the spectra. However, the calculated data are systematically lower than the measured results for the detector at 198.5 cm. For the detector at the greater distance, the comparison is quite favorable.

In both comparisons, it can be noted that the calculation does not reproduce the slope in the differential spectra between ∿2 and 4 MeV. This anomaly is being investigated. The data agree within a factor of ∿2 or less over the neutron energy range from 850 keV to 15 MeV.

The differential and integral gamma ray spectra are compared in Fig. 16. The calculated data are lower than the measured results at all gamma ray energies. This disagreement seems to indicate that the gamma ray production cross sections for the components of Hevimet are not as well established as those of stainless steel and borated polyethylene.

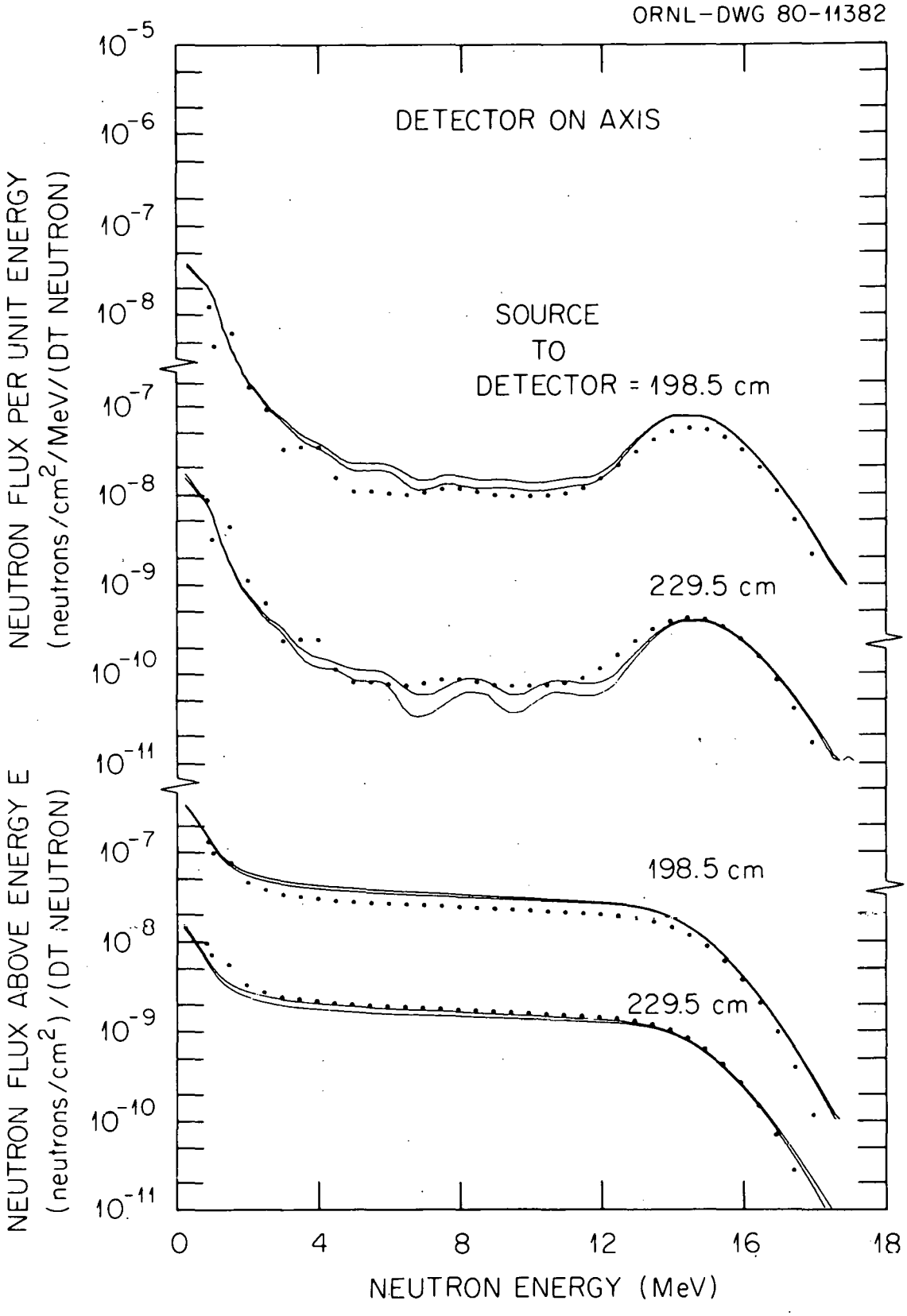

Fig. 15. Neutron flux per unit energy and neutron flux above energy E vs. neutron energy for the slab containing hevimet as a function of source-to-detector distance on axis.

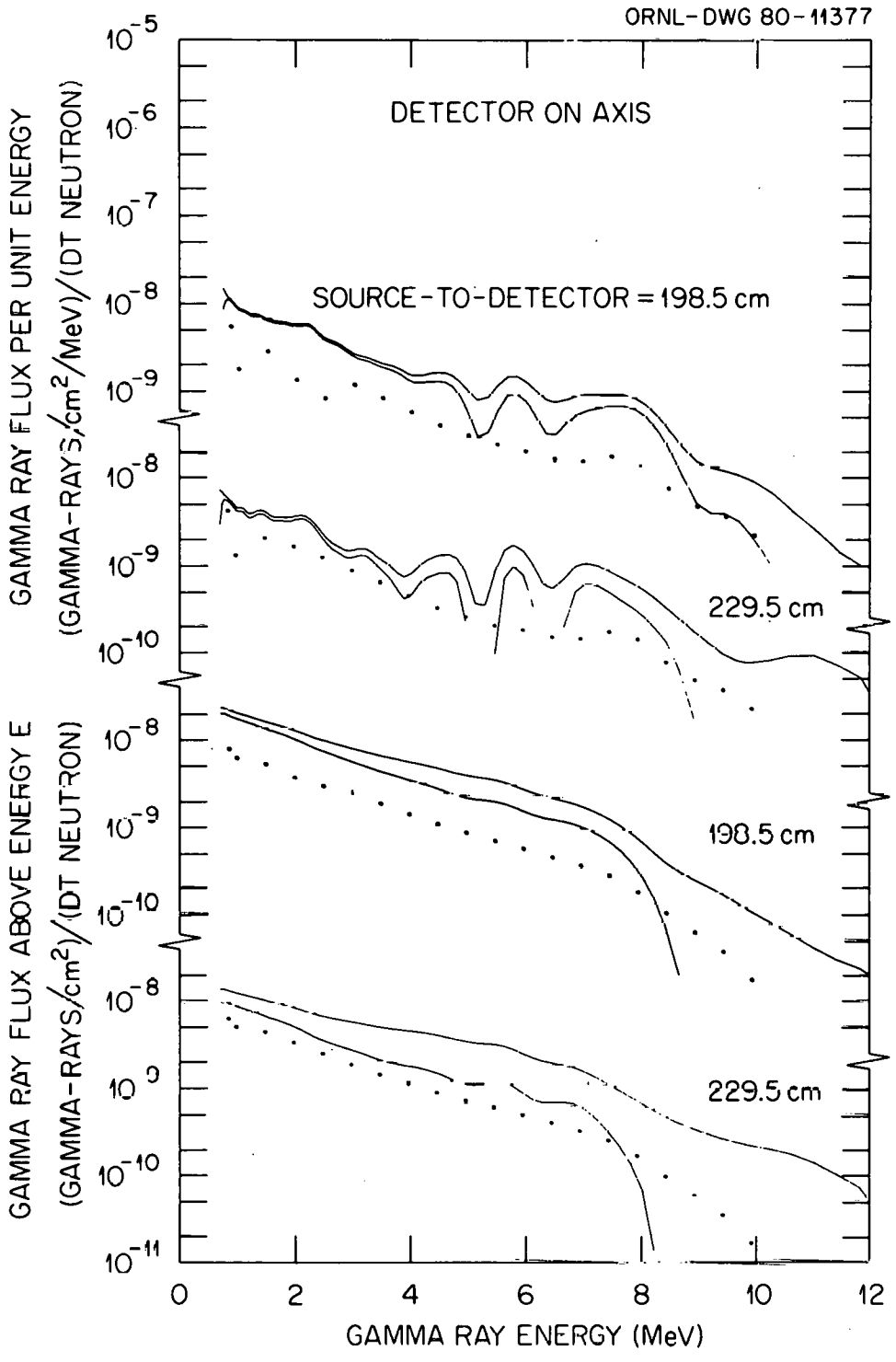

Fig. 16. Gamma ray flux per unit energy and gamma ray flux above energy E vs. gamma ray energy for the slab configuration containing hevimet as a function of source-to-detector distance on axis.

Since the gamma ray spectra compare more favorably for configuration 5 (see Table IV and Fig. 10) when the Hevimet is not present, it can be concluded that the disagreement between the measured and calculated spectra arises from the Hevimet.

IV. CONCLUSIONS

The calculated and measured neutron and gamma ray energy spectra compared here suggest that two-dimensional discrete ordinates methods in combination with ENDF/B-IV cross section data are satisfactory for the analysis of 14-MeV neutron transport through fusion reactor shields when the slabs are comprised of SS and BP and for the thicknesses and compositions given in Table IV, the calculated neutron energy spectra are in good agreement with those obtained from measurements. The agreement is less favorable when Hevimet is included as a shield material. The gamma ray spectra are, for the most part, in good agreement particularly in magnitude. The structure in the measured gamma ray spectra are not reproduced. The calculated gamma ray spectra behind slabs containing Hevimet are in poor agreement with the measured spectra which suggests that the gamma ray production cross section data for components of this material may require further evaluation.

REFERENCES

1. G. T. Chapman, G. L. Morgan, and J. W. McConnell, "The ORNL Integral Experiments to Provide Data for Evaluating the MFE Shielding Concepts. Part I: Attenuation Measurements" ORNL/TM-7356, Oak Ridge National Laboratory (to be published).
2. R. T. Santoro, J. M. Barnes, R. G. Alsmiller, Jr., E. M. Oblow, "Calculational Procedures for the Analysis of Integral Experiments for Fusion Reactor Design," ORNL/TM-7094 (to be published).
3. E. M. Oblow, "DMFE Integral Experiment Progress Report 10/76-10/77" Oak Ridge National Laboratory (unpublished).
4. W. R. Burrus and V. V. Verbinski, Nucl. Instr. Methods 67, 181 (1979).
5. R. W. Roussin, C. R. Weisbin, J. E. White, N. M. Greene, R. Q. Wright, J. B. Wright, "The CTR Processed Multigroup Cross Section Library for Neutronics Studies," ORNL/RSIC-37, Radiation Shielding Information Center, Oak Ridge National Laboratory (1975); also available as DLC-41.
6. W. W. Engle, Jr. "A User's Manual for ANISN, A One-Dimensional Discrete Ordinates Code with Anisotropic Scattering," K-1693, Oak Ridge National Laboratory (1967).
7. "BUGLE, Coupled 45 Neutron, 16 Gamma Ray, P_3, Cross Sections" for Studies by the ANS 6.1.2 Shielding Standards Working Group on Multigroup Cross Sections," DLC-47, Radiation Shielding Information Center, Oak Ridge National Laboratory (1977).
8. R. A. Lillie, R. G. Alsmiller, Jr. and J. T. Mihalczo, Nucl. Technol. 43, 373-381 (1979).
9. W. A. Rhoades and F. R. Mynatt, "The DOT III Two-Dimensional Discrete Ordinates Transport Code," Oak Ridge National Laboratory, ORNL/TM-4280, (1979).

ORNL/TM-7360
Dist. Category UC-20d

Internal Distribution

1-2. L. S. Abbott
3. F. S. Alsmiller
4-8. R. G. Alsmiller, Jr.
9. J. Barish
10-11. J. M. Barnes
12. D. E. Bartine
13. L. A. Berry
14-15. G. T. Chapman
16. T. A. Gabriel
17. H. Goldstein (Consultant)
18. R. A. Lillie
19. F. C. Maienschein
20. E. M. Oblow
21. R. W. Peelle
22. R. W. Roussin
23. M. W. Rosenthal
24. RSIC
25-29. R. T. Santoro
30. D. Steiner
31. C. R. Weisbin
32. G. E. Whitesides
33. A. Zucker
34. P. Greebler (Consultant)
35. W. B. Loewenstein (Consultant)
36. R. Wilson (Consultant)
37-38. Central Research Library
39. ORNL Y-12 Technical Library
Document Reference Section
40. Laboratory Records Department
41. ORNL Patent Office
42. Laboratory Records - RC

External Distribution

43. Office of Assistant Manager, Energy Research and Development, DOE-ORO, Oak Ridge, TN 37830
44. J. E. Baublitz, Office of Fusion Energy, Division of Development and Technology, MS G-234, U.S. Department of Energy, Washington, DC 20545
45. F. E. Coffman, Chief, Systems and Applications Studies Branch, Office of Fusion Energy, U.S. Department of Energy, Washington, DC 20545
46. B. Engholm, General Atomics Company, P.O. Box 81608, San Diego, CA 92138
47. C. R. Head, Office of Fusion Energy, MS G-234, U. S. Department of Energy, Washington, DC 20545
48. R. Ng, Office of Fusion Energy, U.S. Department of Energy, Washington, DC 20545
49. P. Sager, General Atomics Company, P.O. Box 81608, San Diego, CA 92138
50. Dr. Yasushi Seki, Japan Atomic Energy Research Institute, Tokai-mura, Ibaraki-ken, Japan
51-188. Given distribution as shown in TID-4500, Magnetic Fusion Energy (Distribution Category UC-20d: Fusion Systems)